Applied Catalysis B: Environmental 181 (2016) 279–288

Contents lists available at ScienceDirect

Applied Catalysis B: Environmental

journal homepage: www.elsevier.com/locate/apcatb

Iron phthalocyanine and MnOx composite catalysts for microbial fuel cell applications

Richard Burkitt*, T.R. Whiffen, Eileen Hao Yu*

School of Chemical Engineering and Advanced Materials, Merz Court, Newcastle University Newcastle Upon Tyne, NE1 7RU, United Kingdom

ARTICLE INFO

Article history:
Received 22 November 2014
Received in revised form 29 May 2015
Accepted 7 July 2015
Available online 17 July 2015

Keywords:
Microbial fuel cell
Oxygen reduction reaction
Iron phthalocyanine
Manganese dioxide
Disproportionation

ABSTRACT

A low cost iron phthalocyanine (FePc)-MnOx composite catalyst was prepared for the oxygen reduction reaction (ORR) in the cathode of microbial fuel cells (MFCs).

The catalysts were characterised using rotating ring disc electrode technique. The *n* number of electrons transferred, and H_2O_2 production from ORR was investigated. The FePc–MnOx composite catalyst showed higher ORR reduction current than FePc and Pt in low overpotential region. MFC with composite catalysts on the cathode was tested and compared to Pt and FePc cathodes. The cell performance was evaluated in buffered primary clarifier influent from wastewater treatment plant. The membrane-less single chamber MFC generated more power with composite FePcMnOx/MON air cathodes (143 mW m^{-2}) than commercial platinum catalyst (140 mW m^{-2}) and unmodified FePc/MON (90 mW m^{-2}), which is consistent with the RRDE study.

The improvement was due to two mechanisms which abate H_2O_2 release from the composite. H_2O_2 is the reactant in two processes: (i) chemical regeneration of MnOx after electro-reduction to Mn^{2+}, and (ii) peroxide undergoing chemical disproportionation to O_2 and H_2O on an electrochemically aged manganese surface retained in the film. Process (i) has the potential to sustain electrochemical reduction of MnOx at cathode potentials as high as 1.0 V_{RHE}.

1. Introduction

Microbial fuel cell (MFC) technology combines the developments in the biotechnology and fuel cell sectors. This fusion of capabilities gives MFCs a unique niche. One area of growing interest is waste water treatment. Pilot scale bio-electrochemical systems have been constructed and operate with the primary aims of (a) organic pollutant removal, quantified by a decrease in chemical oxygen demand (COD), and (b) the aim of energy recovery in the form of electricity or H_2 production. Several pilot scale MFCs have been constructed. The first large-scale test of MFCs was conducted at Foster's brewery in Yatala, Queensland in 2009. The tubular shaped MFC contained 12 modules with 3 m height each, with a total volume approximately 1 m^3. The performance of the MFC was not known,but the current generation was low due to low conductivity of the brewery wastewater [1]. The first microbial electrolysis cell (MEC) for hydrogen production was set up at the Napa Wine Company, USA, also in 2009 [1]. Another pilot scale MEC for hydrogen production was conducted in a wastewater treatment plant (Northumbrian Water) by researchers from Newcastle University, UK. The MEC produced hydrogen 0.015 L day^{-1} for more than 12 months [2]. More recently a stackable domestic wastewater MFC in Harbin, China [3] removed 79% of COD at 0.116 W for electrolyte volume of 250 L.

In an MFC, bacteria immobilised on the anode oxidise organic matters to CO_2 from the wastewater stream. Electrons and protons are produced from the oxidation. The carbon anode functions as a solid electron acceptor, and physical support to the bacteria. On the cathode, oxygen reduction reaction (ORR) occurs with oxygen as the electron acceptor receiving electrons transferred through external circuit, and combined with protons produced from anode transferred through the electrolyte. A cathode opens to the atmosphere, minimising the oxygen mass transfer limitation. This is a common configuration known as air cathode. Oxygen adsorbed on the surface of an electrocatalyst functions as the terminal electron acceptor ($E^{0'}$ = 1.223 V RHE, pH 7) for electrons sourced from the anode.

Traditionally platinum catalyst has been used for oxygen reduction reactions in the cathodes. Oxygen reduction occurs at low overpotential on the Pt surface, around 1.05 V (RHE, pH7). The high price of Pt makes it unfeasible for use in the MFC [4]. Low cost

* Corresponding authors. Fax: +44 191 222 5292.
E-mail addresses: richard.burkitt@gmail.com (R. Burkitt), eileen.yu@ncl.ac.uk (E.H. Yu).

http://dx.doi.org/10.1016/j.apcatb.2015.07.010

alternatives in development include transition metal macrocycles [5–7], manganese oxide [8,9] and modified carbon materials [10]. Carbon materials facilitate the two electron pathway for O_2 reduction at a large overpotential, producing H_2O_2, an oxidising agent with a high formal potential ($E^{0'}$ = 1.76 V vs. RHE). This makes H_2O_2 incompatible with oxidation sensitive metallo-organic electro-catalysts and ion exchange membranes. In anion exchange membranes tertiary amine groups are susceptible to H_2O_2. The presence of Fe^{2+} in wastewater creates Fenton's reagent ($^{\bullet}OH$) from peroxide. $^{\bullet}OH$ greatly exacerbates $SO_3{}^{2-}$ and F^- release from substitution reactions in proton exchange membranes and can reduce mechanical rigidity in anion exchange membranes from reactions on the backbone.

$$O_2 + 4e^- + 2H_2O \rightarrow 4OH^- \left(E^{0'}_{pH7} = +1.224 V vs. RHE\right) \quad (1)$$

$$O_2 + 2H^+ + 2e^- \leftrightarrow H_2O_2 \left(E^{0'}_{pH7} = +0.696 V \text{ vs. RHE}, pO_2 = 0.2, [H_2O_2] = 5 mM\right) \quad (2)$$

$$H_2O_2 + 2e^- + 2H^+ \rightarrow 2H_2O \left(E^{0'}_{pH7} = +1.764 V vs. RHE, [H_2O_2] = 5 mM\right) \quad (3)$$

In an MFC, iron phthalocyanine (FePc) shows comparable or higher ORR activity to Pt [11,12], proceeding via four-electron transfer [13,14]. Most studies focus on a form of chelated iron, produced from pyrolysis of carbon supported FePc [6,7,13]. This approach was used in previous studies due to early work establishing that pyrolysis enhances stability in acidic media [15]. The pyrolysis step embeds iron and chelating nitrogen into graphite planes, forming a variety of covalently bonded FeNx sites (such as $FeN_2C_2{}^-$ and $FeN_3C_2{}^-$) intercalated into the graphite sheet [15]. The activity of the pyrolysed sites is a function of pyrolysis time, temperature, coverage and carbon support.

Although pyrolysis is a common procedure for metal macrocycle catalysts, in which it is supposed to improve the stability of the metal macrocycles [15], pyrolysis produces an array of metal intercalated catalytic sites with different formal potentials and activities. Previous studies have shown that un-pyrolysed FePc has a high degree of activity and stability in neutral media. In [16–18], the authors highlight the benefits of avoiding the energy intensive process of catalyst pyrolysis. For instance, Baranton et al. [19] demonstrate Me–O_2–Me bridging chemistry positively influences kinetics. This depends on Me–Me separation, at temperatures high enough to decompose FePc [15] these crystalline deposits are largely lost and the majority of sites react with O_2 independently from each other, reducing the number of possible ORR reaction pathways. In a separate study, our results have indicated that pyrolysis significantly degrades the loading of potential catalytic sites by upto 96%, with no improvement in ORR kinetics [20]. Our study omits the pyrolysis step to allow a chemically homogenous FePc catalytic site to be in contact with the electrolyte. Two main mechanisms of FePc deterioration have been identified. Demetallation, Eq. (4), O_2 binds strongly to the heme dislocating the iron from the flat macrocycle plane. This oxo-adduct is then susceptible to substitution of the ferric ion with two protons, producing H_2Pc [20–22]. Deactivation by reactive oxygen species (ROS) such as trace H_2O_2 cause FePc site deactivation [22] by forming $^{\bullet}OH_{(ads)}$ upon H_2O_2 adsorption and passivizing the macrocycle via Eq. (5) [23]. In the study of Chen et al., this product $^{\bullet}OH_{(ads)}$ was partially reversible, and activity is regained when the electrode is set to OCP. Demetallation is fast at low pH [22], and ROS deactivation dominates in alkali conditions [23].

$$2H^+ + FePc - O_2^- \rightarrow H_2Pc + Fe^{2+} \quad (4)$$

$$H_2O_2 + FePc \rightarrow FePc(OH)_{2-\chi} + \chi \bullet OH \; (\chi = 0 or 1) \quad (5)$$

Suppressing H_2O_2 production has been the aim of composite catalyst systems comprised of a macrocycle and transition metal oxide element, most notably MnOx [24–27]. Solid Mn(IV) minerals have been applied in MFC cathodes, functioning as catalysts or terminal electron acceptors depending on the solution pH [8,9,28–32]. Roche et al. studied ORR in alkaline media using manganese oxides (MnOx). The MnOx catalyst was also implemented in an MFC with artificial wastewater obtaining a power density of <200 mW m^{-2} [33]. An initial reduction step involving proton insertion produced MnOOH, a form thought to be ORR active; thus, producing a reduction wave with Tafel slope of $-b_c$ = 0.153 V dec^{-1} at pH 7 [33]. There is discord on the nature of MnOx upon cathodic polarisation, as a current can be observed without oxygen [9]. Mediator mechanisms involving continual cycling between Mn^{4+} and Mn^{3+} have been postulated [28,34], suggesting Mn^{3+} possibly reduces O_2 to H_2O by a series of single electron transfers in solution. This requires soluble Mn forms which are subject to leaching. Combining MnOx with another non-precious ORR catalyst may achieve sustainable ORR if the other catalyst is susceptible to de-activation by accumulated H_2O_2, as is the case with FePc in Eq. (5).

Previously composite catalyst systems have utilised cobalt porphyrins due to the higher formal potential of the Co(I)/Co(II) redox [14] than equivalent Fe(II)/Fe(III) macrocycles. Although ORR is initiated at a higher potential in the cobalt systems, the H_2O_2 release is significant. This is partially abated with the co-deposition of metal oxides in the catalyst film. Prioritising both minimum H_2O_2 release and minimum cost [20] leads us to study iron phthalocyanines in a co-catalyst system. For a synergistic interaction between the FePc and metal oxide component, a small spacing molecular spacing (c.a. Å) between the Mn–O and Fe–N component is required. A simultaneous co-deposition approach to the MeOx and FePc components may produce the highest proportion of binary catalyst sites in close proximity. A method of simultaneous solvent co-deposition has never been attempted to the best of the authors knowledge. Instead, two consecutive deposition steps for macrocycle then MnOx is favoured [24–27,35], in thin sequential thin films [24,25,27], or supported on carbon [26,35].

Composite catalysts with cobalt-tetramethoxyphenylporphyrine (CoTMPP) deposited from pyridine solution onto manganese oxide were prepared by Xie et al. [26]. An array of MnOx forms were confirmed with XRD upon pyrolysis. The 800 °C heat-treated composite produced the highest ORR current in an alkali electrolyte zinc–air battery. Rotating ring disc electrode (RRDE) technique was not employed; therefore, no link could be drawn between MnOx crystalline type and H_2O_2 decomposition rate. Arihara et al. [24] treated a glassy carbon disc with cobalt phthalocyanines. Variants of the cobalt phthalocyanine examined were those with or without (a) an axial cyanide ligand or (b) 16 fluoride atoms on macrocycle ring periphery. These modifications greatly influenced catalytic activity. The macrocycles were deposited from dimethylformamide, to which vacuum dried product an MnOx-Nafion slurry was applied. The CoPcCN–MnOx resulted in a decreased ring current compared to CoPcCN in RRDE experiments, indicating less H_2O_2 was released from the disc to be oxidised at the ring. This was attributed to H_2O_2 decomposition by MnOOH. In dilute H_2SO_4 media, El-Deab et al. [25] used RRDE to study non-pyrolysed CoTMPP-MnOx nanoparticle composites. Electrogenerated MnOx was coated with CoTMPP from equilibrium adsorption from dimethylformamide. They noted that, MnOx addition increased disc current and reduced ring current. Their explanation was an enhanced rate of peroxide disproportionation, present in other co-catalyst systems [35]. The disproportionation reaction, Eq. (6), can be promoted by an unpolarised heterogeneous catalyst surface, with reaction schemes for metal oxides proceeding along paths similar to Eqs. (7) and (8). When occurring on a catalyst surface, the rate of Eq. (6)

is invariant of applied potential [36], provided catalyst surface phase metal oxide chemistry is invariant over the potential range under consideration. Physical characterisation ranges from SEM to XRD (on MnOx). Overall, no direct influence of the MnOx on the macrocycle heme has been identified with XPS or electrochemical methods. ORR occurs at the same potential with or without MnOx indicating a decomposition/reduction reaction [37–39] which occurs after H_2O_2 formation and diffusion. Previous studies indicate certain MnOx forms may be suitable for H_2O_2 degradation [40], possible pathways and chemical regenerative reactions are listed below in Eqs. (6)–(12) [41,42]. At pH 7.0, the hydrolysis of water co-ordinating Mn^{3+} is significantly faster than that of $Mn^{2+}{}_{(aq)}$ [42]. The presence of electrogenerated H_2O_2 may assist in regenerating $Mn^{3+}{}_{(aq)}$ and in turn the solid Mn(IV) Ox. The direct regeneration of Mn(IV) from reactions between Mn^{2+} and O_2 is negligible. Establishing catalytic activity for H_2O_2 decomposition following polarisation is a primary aim of this investigation.

$$H_2O_2 + H_2O_2 \rightarrow O_2 + 2H_2O\,(\text{slow}) \quad (6)$$

$$MnO_2 + H_2O_2 \rightarrow Mn(OH)_2 + O_2\,(\text{fast}) \quad (7)$$

$$Mn(OH)_2 + H_2O_2 \rightarrow MnO_2 + 2H_2O\,(\text{fast}) \quad (8)$$

$$2Mn^{2+} + H_2O_2 + 2H^+ \rightarrow 2Mn^{3+} + 2H_2O \quad (9)$$

$$[Mn(H_2O)_6]^{3+} \leftrightarrow [Mn(H_2O)_5OH]^{2+} + H^+ pK_a = 0.2 \quad (10)$$

$$[Mn(H_2O)_6]^{2+} \leftrightarrow [Mn(H_2O)_5OH]^{+} + H^+ pK_a = 10.59 \quad (11)$$

$$[Mn(H_2O)_5OH]^{2+} \rightarrow MnOOH + 2H^+ \quad (12)$$

In this study, carbon supported composite catalysts of FePc–MnOx have been prepared as air cathodes and characterised in half-cells containing phosphate buffer (PBS). The scope of this study extends to the performance of designs that can feasibly be used in MFC's treating organic contaminants in wastewater streams. To achieve the aim, polarisation of these air cathodes is performed in MFCs filled with wastewater collected from primary clarifier influent at a treatment plant near Newcastle, UK.

2. Material and methods

2.1. Catalyst preparation

60 wt.% Iron phthalocyanine (FePc) supported on carbon was prepared by deposition from concentrated H_2SO_4 as described previously [6]. Carbon Monarch 1000 (Cabot) support was used for FePc and the pyrolysis step omitted. After FePc deposition, catalysts were filtered and the filter cake repeatedly washed with de-ionised water until the filtrate was pH > 5 and the majority of H_2SO_4 removed. 1 g of the resulting powder (FePc/MON) was treated with 11.83 mg of $MnSO_4$ in 70 mL H_2O (Analytical grade, VWR) under N_2 for 40 min followed by dropwise addition of 30 mL of 33 mM $KMnO_4$ (98%wt. VWR) solution under N_2 and temperature control at 80 °C [33]. This caused excessive $KMnO_4$ surface oxidation ($[MnO_4^-] > [Mn^{2+}]_{ads}$) depositing MnO_2. Monarch 1000 has received a factory treatment of concentrated HNO_3 [8], creating diverse nucleation sites for MnO_2 deposition. For simplicity, this catalyst is referred to as FePcMnOx/MON. After synthesis catalysts were then washed at room temperature in H_2O with twenty batch equilibrium desorption washes. XPS analysis on Fe2p and N1s showed the effective %FePc wt. to be 5.87–6.98% in FePc/MON and 4.11–9.87% in FePcMnOx/MON. Chemicals were analytical grade unless otherwise stated. 20% Pt/C (Alfa Aesar) was used as a benchmark catalyst.

2.2. XPS analysis of catalyst powders

Catalysts produced in Section 2.1. are pressed onto a carbon loaded SEM sticky pad for XPS. A Thermo K-Alpha XPS system subjected samples to monochromatic X-rays from a filtered aluminium anode at 50 eV pass energy. Peak half width maximums ($W_{1/2}$) of individual transmissions are expressed in eV. Analysis was performed using CASA XPS software and is described in Appendix A of Supplementary file.

2.3. Half-cell tests with gas diffusion electrodes

2.3.1. Air (working) electrode preparation

A catalyst ink consisting of 2 ml of ethanol, 20 mg of catalyst and 43 μL of Nafion (5%wt.) ionomer (Sigma) was ultrasonicated at room temperature for 30 min to colloid consistency. The weight percentages of Nafion:FePc + MnOx + C ratio of 9.8%. The resulting ink was painted on to Wet proofed carbon Toray 90® paper electrodes (1 cm diameter) until desired loading achieved. The electrodes were hot pressed at 130 °C for 3 min at 50 kg cm^{-2}. FePc, FePcMnOx/MON and Monarch carbon catalyst powders were applied to a total weight of 1.6 mg cm^{-2}. Platinum metal loading was 0.5 mg cm^{-2} (Alfa Aesar 20 %wt. Pt). Working electrodes were fixed into the gas diffusion Cell (GDC) with silicon gaskets reducing the area in contact with the electrolyte to 0.2826 cm^2 which was the basis for all calculations.

2.3.2. Electrochemical characterization in gas diffusion cell (GDC)

Electrochemical study of GDC in a three-electrode cell consisted of the air cathode as working electrode, a Pt foil counter electrode and a ceramic frit Ag|AgCl 3 M NaCl reference electrode, BASi-RE6. All potentials are converted to vs. a reversible hydrogen electrode (RHE) which is calculated from Eq. (13).

$$E_{RHE} = E_{vs.Ag|AgCl} + 0.059pH + 0.208 \quad (13)$$

where E_{RHE} would be the measured potential vs. a reversible hydrogen electrode (in pure pH7 solution), $E_{vs.Ag|AgCl}$ is the experimentally measured potential vs. a fresh Ag|AgCl reference electrode. 0.208 V is the formal potential of an Ag|AgCl electrode with 3 M NaCl filling solution at 25 °C vs. NHE.

A quartz filter (5 μm pore) was placed between working electrode and counter to reduce cross-over of gases from water splitting. Electrodes were spaced 4 cm, and the reference luggin tip was 2 mm from the working electrode surface. All parameters (P and J) were calculated based on wetted geometric area 0.283 cm^2. The exchange current (J_0) was reported based on geometric area, rather than electroactive surface area. Electrochemical surface area (for Pt) and turnover rate per site (FePc) could be used to report equilibrium activity more accurately. Measurements were performed by an Autolab PGSTAT303 (Eco Chemie) potentiostat using automatic current ranging in voltammetric experiments.

Gas diffusion cells were filled with 50 mM of Na^+ phosphate buffer solution (PBS) (Sigma–Aldrich), pH 7.0 at 5.5 < mS cm^{-1} < 6. Open circuit potential (OCP) was recorded at t = 16 h in quiescent air saturated 50 mM PBS, followed by ten consecutive cyclic voltammograms at potential scan rate υ = 20 mV/s. linear sweep voltammograms (LSV) at υ = 1 mV/s are then used to quantify ORR activity.

2.4. Inductively coupled plasma (ICP) analysis of electrolytes after polarization of MnOx electrodes

Air cathodes (4 cm^2) of MnOx/MON with catalyst loading 1 mg cm^{-2} were prepared with 10%wt. PTFE binder. Both electrodes were immersed in N_2 saturated 50 mM PBS. One was left at open

circuit (without consecutive CV) whilst another was subjected to repeat CV until stable featureless capacitive profiles are obtained [43]. The electrolyte was then filtered through 0.45 μm syringe filters and sent for ICP analysis. The results are presented in Table 2 using the same MnOx/MON loading calculations mentioned above.

2.5. Single chamber microbial fuel cell

2.5.1. Preparation of electrodes

Larger versions of the air cathodes mentioned in Section 2.3.1 (19.63 cm^2) were prepared and sealed into a single chamber MFC with compressible gaskets reducing the wetted area to 12.56 cm^2. A carbon felt anode 1.27 cm thick (Alfa Aesar) was inoculated with primary clarifier influent from Cramlington treatment works, UK. The enrichment medium contained (40 mg/L NH_4Cl, 10 mg/L $MgCl_2$, 5 mg/L $CaCl_2 \cdot 2H_2O$, 0.1 mg/L $MnSO_4 \cdot 4H_2O$, 0.1 mg/L $CuSO_4 \cdot 5H_2O$, 0.1 mg/L $ZnCl_2$), wastewater, phosphate buffer solution (PBS) and 1 g/L sodium acetate. The anode was connected with a Ti wire (Alfa Aesar) and a potential of $E = 0.422$ V (RHE) was applied [44] until 500 mA m^{-2} electrogenic current was obtained. A platinum counter electrode was used during biofilm growth. Two cycles in wastewater/PBS (no acetate) were performed with a fixed resistor (R_{ext} = 1 kΩ) to remove CH_3COONa then the appropriate FePcMnOx/MON, FePc/MON or Pt/C air cathodes were inserted.

2.5.2. MFC tests with wastewater

The architecture of microbial fuel cells has been described [20] and is depicted in the appendix, Fig. A.1a of Supplementary file. Briefly, three Perspex sections fit together to place the cathode under tight compression using screws and bolts with silicone gaskets. The leak tested single chamber has an anode–cathode separation of 3.2 cm and filled volume 38 ml. Primary clarifier influent was stored at 4 °C and used within a week of collection. Primary clarifier influent (75%v/v) was amended with (25 %v/v) 200 mM PBS stock solution to ensure conductivity and to eliminate cathode alkalisation from ORR. The buffered wastewater was sparged with N_2 and placed into the cell. Polarisations were performed with a data logger monitoring electrode potentials (Pico Log ADC 16). During open circuit, O_2 diffusion into the cell was controlled by covering the air cathode with Parafilm and removed upon connecting the resistor. This was done to maintain anaerobic conditions at the anode which can occur, when starting membraneless MFC systems. Cells were placed at OCP for 16 h prior to polarisation curves and during electrolyte change.

Polarisation curves were obtained with resistor substitution boxes (RS 500 Elenco Electronics) which were connected first at 1 MΩ and then stepped down every 20 min. 14 distributed resistance values from 1 MΩ to 50 Ω were used. The stabilised V_{cell} and E_{cat} were recorded after 20 min before fixing the next resistance value. Upon completion of polarisation curves the MFCs were operated on a fixed resistor (R_{ext} = 1 kΩ). In the MFC, a salt bridge sheath (KCl:Agar = 1:4 wt. basis) was added to prevent reference electrode drift (Fig. A.5b of Supplementary file). The salt bridge sheath prevented drift of more than 30 mV over all wastewater cycles. Current density and power density were calculated as in Eqs. (14) and (15).

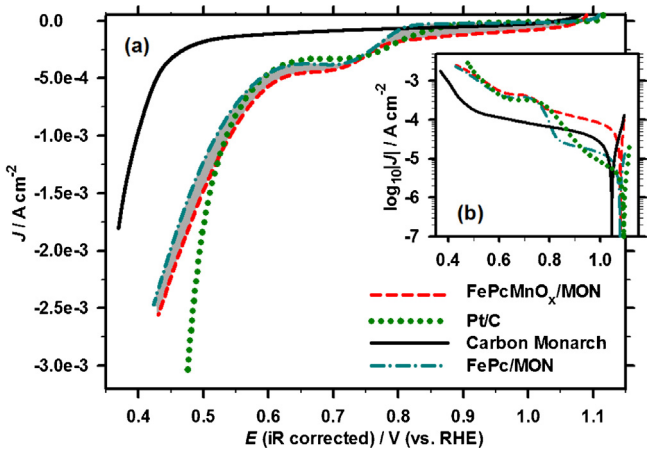

Fig. 1. (a) LSV of air cathodes after brief aging. (b) Inset shows logarithmic current against iR corrected potentials, grey area shows increased current in new air cathodes from MnOx incorporation. υ = 1 mV s^{-1}. Electrolyte; 50 mM PBS, pH 7.0.

$$J = \frac{V_{cell}}{R_{ext} \times A_{an}} \quad (14)$$

$$P = \frac{V_{cell}^2}{(R_{ext} \times A_{an})} \quad (15)$$

where J = current density (Amps cm^{-2}), V_{cell} = cell voltage (Volts), R_{ext} = external resistance (Ohms) and A_{an} = projected anode area (25 cm^2).

3. Results and Discussion

3.1. O_2 reduction activity of gas diffusion electrode in half cells

The electro-catalyst performance in gas diffusion electrodes was summarised in Table 1. A solution resistance (R_s) of 290 Ω was obtained with electrochemical impedance spectroscopy performed on the GDE. All *i–E* data in Fig. 1 and Table 1 was post-measurement iR-drop corrected by 290 Ω. Linear regression of cathodic tafel slopes (from $\log_{10}(J)$ vs. E plots such as Fig. 1b) to the OCP recorded prior to polarisation was use to obtain the corresponding exchange current reported (J_0). The number of redox active FePc sites per geometric area (RAS) on the electrode is quantified by charge integration of Fe(II) Pc/Fe(III) Pc oxidation peak in de-aerated medium from 5 mV/s cyclic voltammetry (CV). This technique is adapted from analysis of FePc in H_2SO_4 [21] and KOH [45] electrolytes. A control test for carbon contaminants was performed using cyclic voltammetry on Monarch carbon treated with conc. H_2SO_4. This control test showed the Fe(II)/Fe(III) peak to be absent, indicating the redox peak was not related to iron contaminants present in the untreated carbon black.

Table 1
Summary of air cathode performance υ = 1 mV/s. Electrolyte; 50 mM PBS, pH 7.0.

Catalyst	Tafel Slope, $-b_c$ (iR corrected)		J_0 (geo.) A cm^{-2}	E_{onset}/V_{RHE}	RAS × 10^{15} cm^{-2}	J_{WE} @ 0.522 V mA cm^{-2}	E @ -0.4 A m^{-2}/V_{RHE}	OCP (16 h)/V_{RHE}
	Process	V dec^{-1}						
$FePcMnO_x/C$	MnO_x reduction	−0.59	7.8×10^{-5}	0.459	9.9	−1.21	1.086	1.003
	ORR wave(by Mn-FePc)	−0.19	1.3×10^{-5}					
FePc/C	ORR wave (by FePc)	−0.0675	8×10^{-8}	0.457	7.4	−0.984	0.822	1.002
Monarch	$2e^-$ ORR wave	−0.103	1.5×10^{-7}	0.425		−0.155	0.439	0.804
Pt	2nd Tafel region	−0.124	2×10^{-6}	0.471		−1.24	0.617	1.023

Table 2
ICP analysis of polarized MnOx-MON or FePcMnOx/MON modified carbon paper (Toray 90) air cathodes. Area = 4 cm^2. Electrolyte; 50 mM Na^+ PBS, pH 7.0.

Electrode (binder)/electrode polarization?	Mn loading	Electrolyte volume	Total manganese content	Leached mass of Mn from electrode	Proportion of Mn leached from electrode◦
	(mg)	(L)	(ppm)	(mg)	(%)
MnO_x/MON (PTFE) OCP	0.459	0.0188	0.3264	0.00614	1.34
LSV polarised	0.459	0.0188	0.9941	0.01869	4.07
MnO_x/MON (Na^+ Nafion) OCP	0.734	0.0188	0.706	0.01327	1.81
LSV polarised	0.734	0.0188	0.681	0.01281	1.74
$FePcMnO_x$/C (Na^+ Nafion) OCP	0.415	0.0188	1.057	0.01987	4.79
LSV polarised	0.415	0.0188	1.563	0.02938	7.08

Previous studies have set anodic scan potential limits of 0.9 V vs. RHE [19] in acid media as irreversible FePc electropolymerisation may occur at high potentials [46,47]. Oxidation of OH^- facilitates the reaction. It is also possible that one mode of electropolymerisation does not involve a proton/hydroxide ion, in which case similar anodic limits should be set for electrolyte of all pH (vs. aprotic reference reaction in H_2O, such as Ag|AgCl). Therefore, electrodes were not polarised to the O_2/H_2O couple potential of 1.23 V vs. RHE in pH7, but the maximum anodic scan potential of 1.12 V vs. RHE was set for all experiments.

At OCP, the sum of the ORR and MnOx reduction cathodic process produces a combined geometric exchange current of $J_0 = 8 \times 10^{-8}$ A cm^{-2} and 9.1×10^{-5} A cm^{-2} for FePc/MON and FePcMnOx/MON electrodes, respectively. The mixed potential arises from (i) ORR; Eqs. ((1)–(3)) occurring on different catalyst surfaces, and (ii) the MnOx electrochemical reactions that are introduced in a later section on leaching; Eqs. (19) and (20). In FePc/MON, the primary catalyst produces an electron turnover of 0.001 e^- FePc-site^{-1} s^{-1}. Fig. 1a shows a reduction process occurring on FePcMnOx/MON in PBS at high potential. The formation of MnOOH from MnO_2 possesses a suitably high formal potential for this process [32]. With cathodic polarisation, FePc/MON produces a Tafel slope of $-b_c = 0.068$ V dec^{-1}, a process attributed to FePc catalysis of oxygen reduction. ORR reaction kinetics are slower on the unmodified support. Monarch produced a Tafel slope of $-b_c = 0.103$ V dec^{-1}, a relatively fast reaction for carbon black in neutral media [48]. This improvement in kinetics has previously attributed to HNO_3 treatment of the carbon [8,10], a post treatment step in production.

The composite catalyst produced a faradic current at $E = 1.0$ V, with an enhancement over the FePc/MON current of 26.5–11.1% in the applied potential range of 0.7–0.44 V, and a 23–10% improvement over the Pt/C air cathode in the 0.7–0.55 V range. With Pt/C catalyst a c.a. 60 mV dec^{-1} tafel slope is typically observed at low overpotential [6]. Occasionally the transition is between the 60 mV dec^{-1} and 120 mV dec^{-1} slopes is obscured in neutral pH [49]. This is the case in the GDC (Fig. 1b), where, the 60 mV dec^{-1} region is not apparent. At higher overpotential ($E = 0.822$ V), Pt/C catalysed oxygen reduction at $-b_c = 0.124$ V dec^{-1}, a result consistent with previous studies at neutral pH [13].

In Fig. 1a, ORR activity followed the trend FePcMnOx/MON > Pt/C > FePc/MON > Monarch. The increase in cathodic current with MnOx addition to the film is shaded grey. Non-faradic current created a large disparity between onset potential (E_{onset}), where current switches from +ve to –ve current, and the OCP. This was particularly evident in the carbon electrode ($E_{onset} = 1.047$ V, OCP = 0.804 V). Composite FePcMnOx/MON outperforms Pt/C over a wide potential range ($+0.922 > E > 0.522$ V), at lower potential ($E < 0.522$ V) Pt/C outperforms all other electrodes.

$$2(O_2 + 2e^- + 2H^+) \xrightarrow{FePc\ /\ Quinone} H_2O_2 + H_2O_2 \xrightarrow{MnO_x/C} O_2 + 2H_2O$$

Scheme 1. Reaction scheme for indirect 2 electron O_2 reduction to water via disproportionation.

At $E = 0.922$ V, the inclusion of MnOx causes a +469% increase in current. A change in ORR reaction e^-:O_2 stoichiometry would provide an insufficient degree of charge to account for the +469% rise. The $MnO_4^-{}_{(aq)}$ ion has the effect of oxidative etching of graphitic planes [50]. Residual MnO_4^- is removed by successive catalyst washing; therefore, electro-reduction of residual MnO_4^- cannot be the cause of the cathodic current in Fig. 1.

Previous studies on cobalt-macrocycle/MnOx composites universally cite disproportionation (Scheme 1) to explain increases in cathodic current [24,26,27]. The applicability of this explanation to iron-macrocycle/MnOx systems is studied herein at length. Various MnOx polymorphs have proven reactivity with H_2O_2 via Eqs. (6)–(8) [25,51]. The mechanism requires H_2O_2 desorption from the FePc surface [20] for decomposition catalysis by a separate MnOx site to occur. This makes MnOx dispersion relative to FePc an important factor, evaluated by XPS in Section 3.3. When the redox signal from FePc was obtained in de-aerated solutions both FePc/MON and FePcMnOx/MON catalysts delivered a similar quantity of Fe(II)/Fe(III) charge (Table 1, RAS). This indicates that MnOx crystal deposition did not hinder redox activity between the carbon and FePc surface from decreasing the wetted surface area.

3.2. Peroxide decomposition with MnOx composite catalyst

The data in Fig. 2a and b is produced from steady-state voltammograms with convection controlled electrode rotation at 200 rpm. The current obtained on the disc and a poised potential ($E = 1.22$ V vs. RHE) concentric ring are recorded as a function of disc potential. The ratios of the ring and disc currents form the basis of the RRDE method. This method is applied to films of FePc/MON, MnOx/MON, the composite catalyst, the unmodified carbon support and a Pt/C benchmark. Fig. 2a and b shows the relative amount of $2e^-$ and $4e^-$ ORR occurring in the catalyst film, expressed as a value N where the range of N is $2 < N < 4$. N is calculated from Eqs. (A.2) and (A.3) of Supplementary file which results mainly from the ratio of OH^-: H_2O_2 produced in the first instance via Eqs. (1) and (2).

All catalyst films produce a stable CV response in de-aerated media prior to voltammetry in O_2 saturated electrolyte. In Fig. 2a the Monarch carbon support produces mainly H_2O_2 upon onset of ORR ($E < 0.52$ V), in $2e^-$:$4e^-$ proportions which are invariant with potential. The Pt/C benchmark produces primarily H_2O/OH^-. Proportionally more H_2O_2 is produced as the applied potential decreases, an observation consistent with studies in alkaline media [27]. In contrast, the FePc/MON thin film produces proportionally

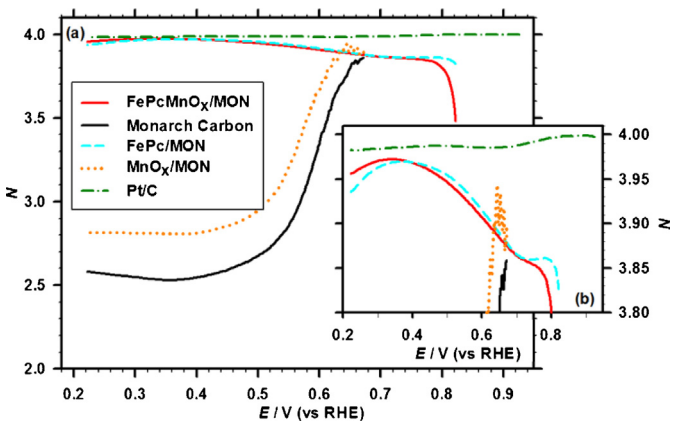

Fig. 2. (a) Proportion of 2/4e⁻ ORR. Thin films applied to 71 μg cm^{-2} with an excess of Nafion binder. Non faradic current has been subtracted. (b) Inset shows enlarged region for *N* values between 3.8 and 4.0. Electrolyte; 50 mM PBS, pH 7.0. ω = 200 rpm. Scan rate; 5 mV s^{-1}.

the most H_2O_2 nearer the Fe(II)/Fe(III) formal potential, an observation consistent with previous studies on FePc [12,13] and Iron pyrrolic/pyridinic chelates [52]. This unusual aspect of FePc catalysis is examined elsewhere [20]. Incorporation of MnOx on the Monarch carbon surface caused an increase in *N* from *N* = 2.5 to *N* = 2.8 at *E* < 0.322 V in Fig. 2a. The MnOx/MON produced 0.57–0.67 times as much disc current as Monarch in this range suggesting 4e⁻ ORR by passivized non-redox active MnOx was not the cause. The geometry of the Monarch and MnOx/MON films is different. The thickness, or distance from GC disc to film-electrolyte interface is thinner for the MnOx/MON film (both 71 μg cm^{-2}), depositing MnOx catalyst decreases the void volume during synthesis. This is particularly relevant as thick films decompose more H_2O_2 prior to release. As the opposite case is seen, this allows one to conclude that MnOx performs significant decomposition catalysis of H_2O_2 over the brief time period where peroxide is retained in the film.

This conclusion is also supported by the comparison of *N*-value for FePcMnOx/MON and FePc/MON in Fig. 2b. There is no noticeable difference in the *N*–*E* profile at high overpotential (0.37 < *E* < 0.7 V), as mainly 4e⁻ are consumed and the disc reaction is relatively slow the overall H_2O_2 amount is small meaning the effect of MnOx catalysis in Eqs. (7) and (8) is a small contribution to the overall current. However, as overpotential increases further still (*E* < 0.37 V) an increase in the overall *N* value is detected in the composite. A comparison of disc currents in this potential range (*E* = 0.3 V) of 2.48 × 10^{-4} A in FePc/MON and 2.52 × 10^{-4} A in FePcMnOx/MON would suggest the reason is not cathodic catalysis but due to improved H_2O_2 disproportionation via Eqs. (7) and (8) reducing the H_2O_2 that leaves the film. Without forced convection the thick film air cathode system incurs a larger H_2O_2 residence time, this is anticipated to make the effect of MnOx on Eqs. (7) and (8) more pronounced.

CV on unmodified Monarch produces a broad redox response associated with quinone [20]. Many quinone groups are capable of catalysing 2e⁻ ORR, with onset potentials as high as *E* = 1.122 V in PBS [53]. Quinones are present in trace quantities in all carbon black materials [54], with varying O_2/H_2O_2 formal potentials. This provides a limited number of tertiary active sites in Macrocycle-MnOx composites. The onset potential of some quinone's may exceed that of $E^{0'}$ of FePc catalysis $E^{0'}$ = 0.78 V [20]. This feature would cause H_2O_2 re-oxidation by FePc at $E > E^{0'}$ [55] or *E* > 0.78 V in pH7, having the effect of nullifying the overall current. Introducing a disproportionation catalyst (such as MnOx) could indirectly produce H_2O before H_2O_2 is re-oxidised at FePc sites or quinone's of lower activity, producing a net cathodic current via Scheme 1. This process may plausibly account for a portion of the enhanced current observed in Fig. 1, another parallel faradic process that contributes to this current is discussed in Section 3.2.

In disproportionation H_2O is the product, however, only two electrons are consumed per O_2 molecule during kinetically limited electro-reduction. At *E* < 0.52 V, the disc current is limited by O_2 diffusion to FePc/MON and FePcMnOx/MON films. The disc current of either film is within +5% of each other at low potential. However, at low potential, Scheme 1 would have negligible effect on current as FePc would directly produce OH^- [20].

3.3. Electrochemical reduction of MnOx in de-aerated media

Leaching of MnOx catalyst is predicted by chemical equilibria data [34], the quantity of electro-reductive dissolution was determined with inductively coupled plasma (ICP) analysis. Eqs. (16)–(20) are pertinent to pH7 media, formal potentials [32] have been adjusted for pH and reference electrode. Carbon paper electrodes were loaded with MnOx/MON and FePcMnOx/MON, with binders of PTFE or neutralised Na^+Nafion. After cathodic polarisation in de-aerated media the spent electrolyte was analysed with ICP. Leached Mn concentrations are summarised in Table 2.

In Table 2, ICP analysis of electrolytes following polarization of both MnOx/MON and FePcMnOx/MON electrodes showed that <7.08% of the initial Mn loading was leached to the electrolyte in all experiments. A small degree of alkalisation (in buffered electrolyte) occurred only in the electrolytes in contact with polarised MnOx electrodes (Table A.1 of Supplementary file). Unpolarised electrodes were only subjected to solution agitation during de-aeration, some Mn leaching occurred (<4.79%).

The amount of Mn leached into the electrolyte following the LSV experiment (Fig. A.2 of Supplementary file) is considered relative to the Mn leached from the unpolarised electrode. The relative rise in Mn leaching caused by cathodic polarisation is +203%, −4% and +48% relative to unpolarised electrodes. Most Mn was retained on the carbon, in contrast to previous works [43]. Therefore, leached Mn was quantified and contrasted with integration of charge passed during cathodic polarisation (Fig. A.2 of Supplementary file) until a stable CV response was obtained. The aim is to ascertain the nature of MnOx redox activity [43,56]. The MnOx/MON and FePcMnOx/MON carbon paper electrodes in Table 2 produced faradic charge of 129 mC cm^{-2} and 73.6 mC cm^{-2}, respectively, until a stabilised response is seen. Using a value of *n* = 2, Eq. (16), this corresponds to 19.95% and 20.18% of initial Mn loading for the MnOx/MON and FePcMnOx/MON electrodes. Comparing this result to Fig. A.2 of Supplementary file, it seems that not all the reduced MnOx makes it into the electrolyte; c.a. 20% of the Mn loading is reduced (without O_2), only 7% makes it into the electrolyte to be analysed by ICP. The contrast between the MnOx/MON Nafion and FePcMnOx/MON Nafion electrodes to polarised leaching in Table 2 may be due to differing quantities of Mn^{2+} being permitted to escape the film prior to reaction with anions such as HPO_4^{2-}, creating solid deposits in the film.

$$MnO_2 + 4H^+ + 2e^- \rightarrow Mn^{2+} + H_2O \quad (16)$$

$$Mn_2O_3 + 6H^+ + 2e^- \rightarrow 2Mn^{2+} + 3H_2O \left(E^{0'}_{pH7} = +0.95 V vs. RHE\right) \quad (17)$$

$$Mn^{2+} + 2OH^- \rightarrow Mn(OH)_2 \quad (18)$$

$$MnO_{2(s)} + H^+ + e^- \rightarrow MnOOH_{(s)} + OH^- \left(E^{0'}_{pH7} = +1.027 V vs. RHE\right) \quad (19)$$

$$MnOOH_{(s)} + 3H^+ + e^- \rightarrow Mn^{2+} \left(E^{0'}_{pH7} = +0.957 V vs. RHE\right) \quad (20)$$

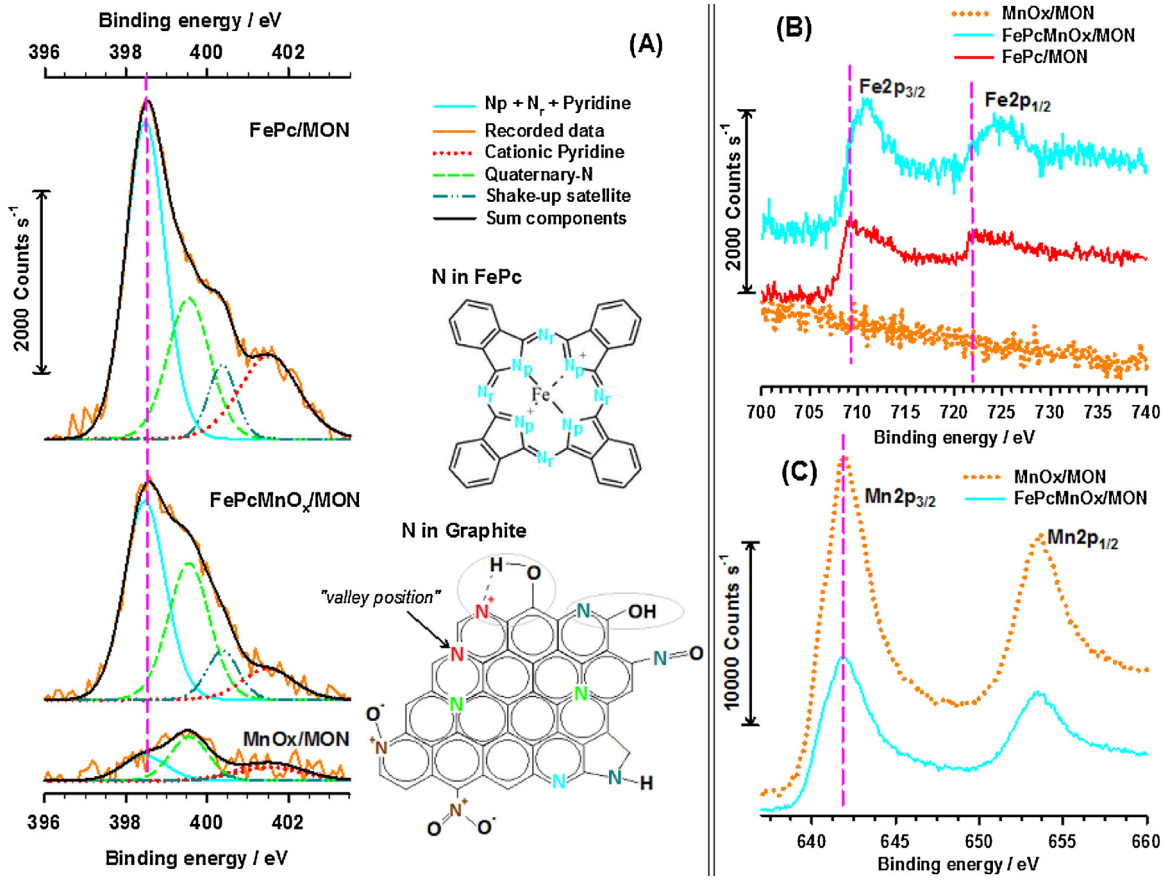

Fig. 3. XPS analysis of (A) N1s spectra, (B) Fe2p spectra and (C) Mn2p spectra of carbon supported composite catalysts. Data treated by (A); Shirley baseline subtraction, or (B) and (C); *Y*-axis re-adjustment of raw data by a fixed CPS amount for each catalyst. Representation of approximate E_B of each nitrogen group [61,62]. Data averaged over four repeat surface samples.

This result suggests mainly electrochemically irreversible surface confined reductive transformation of a portion of MnOx, producing a passivized form in the catalyst layer. This passivized form is redox in-active in the 0.222V < *E* < 1.12 V window. Evidence supporting this assertion appears in the form of stable CV of aged FePcMnOx/MON (Fig. A.4 of Supplementary file), producing x2.97 the charging current compared to FePc/MON. Disproportion activity is retained [57] after electrochemical aging (Fig. 2).

3.4. XPS analysis of composites

The photo-emission energy of metal p-orbital electron after photoexcitation depends on electrophilic interatomic forces exerted on the valence electron cloud. In the case of planar phthalocyanines, the highest occupied molecular orbital of a metal phthalocyanine is directly related to formal potential and the electro-catalytic activity [58]. XPS is used here instead of valence band (low E_B) measurements as different elements frequently overlap in the spectra of crystal organometallics [59], this makes XPS emission spectra easier to consign to certain atoms and easier to calculate relative element presence. XPS is used to evaluate (i) if deposition of each catalyst occurs primarily on separate domains on the carbon surface, (ii) relative surface loading, and (iii) if chelated iron is influenced by MnOx. The photo-emission energy (E_B) following excitation with monochromatic Al X-rays is presented in Fig. 3 for manganese, nitrogen and iron.

Four peaks have been applied to deconvolute the N1s spectra of carbon black supported FePc. Individual photo-emissions correspond to groups of (i) aza and pyrrolic nitrogen in FePc and graphitic pyridinic (light blue), (ii) centre sheet quaternary (light green), (iii) FePc shake-up satellite + graphitic edge plane nitroso, pyridonic and pyrrolic groups (dark blue), and (iv) cationic pyridine (red). Approximate groupings of the E_B recorded in literature [60–63] for each chemical group are colour coded in Fig. 3a. XPS studies with monochromatic Al anode excitation of α-FePc films indicate that all azo (N_r) and pyrrolic (N_p) nitrogen produce similar E_B of only 0.3 eV apart [60,64]. Splitting of these peaks can be observed when FePc is strongly affected by the support material to the planar molecule [64,65]. These amalgamated peaks were consistent in FePc/MON and FePcMnOx/MON, represented by a vertical pink dash line in Fig. 3a. This peak was not deconvoluted further, though the nature is consistent with reported work [60,64] and supported by the stoichiometric atomic ratio of iron–nitrogen, namely ΣFe2p:N1s($N_p + N_r$ only) of 8.79 for FePc/MON, possessing minimal interaction from the graphitic support [64].

The Fe2p spectra is of less analytical use due to the low signal to noise ratio, preventing accurate deconvolution into multiplet sets. However, a clear shift in the $Fe2p_{3/2}$ maxima from E_B = 709.3 eV (FePc/MON) to E_B = 710.8 eV (FePcMnOx/MON) is observed. Only a 24 mV anodic shift in $E^{0'}{}_{FeII/FeIII}$ is observed in Fig. A.4 of Supplementary file with MnOx incorporation, indicating the presence of an additional axial ligand to FePc is implausible. An oxidation state change in chelated Fe could occur from MnO_4^- accepting electrons directly from FePc during sample preparation. The MnOx/MON spectra (Fig. 3c) shows no indigenous iron intercalated into graphite.

The $Mn2p_{3/2}$ signal produces a clear response, a maxima occurred at E_B = 642.08 eV in MnOx/MON and E_B = 641.98 eV in FePcMnOx/MON. This insignificant shift indicates Mn and the phthalocyanine ligand of FePc show no significant interaction. A

Table 3
Atomic prevalence at the catalyst surface by %, determined by XPS.

Catalyst	Carbon	Nitrogen	Iron	Mn	Sulphur	Oxygen (MeOx)	Oxygen (other)
FePc/MON	89.42	2.19	0.16	0.00	0.74	0.00	7.49
FePcMnOx/MON	83.51	1.52	0.23	1.52	0.31	2.57	10.34
MnOx/MON	81.94	0.36	0.00	2.88	0.27	4.81	9.75

Table 4
Summary of air cathode MFC performance with buffered wastewater.

Catalyst	MFC#	OCP		Polarisation		
		Max. E_{cat}/V	Max. V_{cell}/V	P_{max} mW m^{-2}	R_{int} ohms	E_{cat} @ 0.4 Am^{-2}/V
FePcMnO$_x$/C	Cell 2	0.925	0.769	143	381	0.762
Pt	Cell 2	0.911	0.755	140	429	0.732

slight shoulder at E_B = 640 eV is present in both catalysts. This indicates similar MnOx crystals forming in both cases. According to Nesbitt and Banerjee [66], in Mn2p$_{3/2}$ the multiplet with the lowest binding energy is E_B = 641.9 eV ($W_{1/2}$ = 0.87 eV) for an exclusively Mn^{4+} sample, yet it is clear that a lower E_B peak is present indicating Mn^{3+} is present. The relative quantity is difficult to extrapolate from two sets of multiplet photo-emissions, requiring analysis in conjecture with the simpler O1s spectra yields a clearer picture.

Iron Oxide peaks are absent in the O1s spectra (Fig. A.5), this shows that MnO_4^- oxidative treatment of FePc does not result in Iron de-chelation, hence catalytic activity in FePcMnOx/MON is retained (Table 1). The O1s peaks at 531.3 and 533 eV indigenous to the carbon support are slightly increased in samples with MnOx; by 39% in MnOx/MON. This may arise from oxidative action to the carbon by MnO_4^-. At higher pass energies the incident photon can permeate deeper into the surface, however, on the basis of the O^{2-} peak, the proportion of O1s to Mn producing consistent values of "x" in the formula $(Mn^{4+})_{(a)}(Mn^{3+})_{(b)}+(K^+)_{(c)}+(O^{2-})_{(x)}+(OH^-)_{(y)}$ in both samples, being x = 1.6908 in MnOx/MON and x = 1.6910 in FePcMnOx/MON (Table 3) when $a+b$ = 1.0. This preparation method has previously produced a Mn valence of 3.7 [67], compared to the tentative value of 3.392 described in the supplementary information.

The lowest energy emission (E_B = 529.4 eV, $W_{1/2}$ = 1.28 eV) of the O1s photo-emission indicates Mn^{3+}–O^{2-}–Mn^{4+} or Mn^{4+}–O^{2-}–Mn^{4+} which is predicted at 529.6 eV [66]. A minor peak is detected at 530.9 eV from a small gap in the spectra using the fitted peaks, and is attributed to OH^-. The diminutive size of this peak in Fig. A.5 of Supplementary file relative to O^{2-} indicates that manganite (MnOOH) is not formed, but the samples resemble mixed birnessite [68]. This method has previously produced birnessite [67], and the detection (K3s) of trace intercalated K^+ to offset Mn^{3+} in the lattice supports this observation and explains partial reduction of the loaded MnOx in Fig A.2 of Supplementary file.

3.5. MFC performance in wastewater

MFC cell batch performances when operated with composite cathodes in wastewater amended with 50 mM PBS are summarised in Table 4. Total MFC internal resistances (R_{int}) are calculated using the linear ohmic drop region of a V_{cell}–J polarisation curve. Substrate composition and anode fixation were kept consistent. However, in this un-optimized reactor design solution resistance or anode overpotential accounts for the majority of the internal resistance [69]. A similar R_{int} of the MFC operated with FePcMnOx/MON (R_{int} = 381 Ω) and Pt (R_{int} = 429 Ω) cathodes suggests minimal contributions to R_{int} from the catalyst and the semi-conductive coating of MnOx.

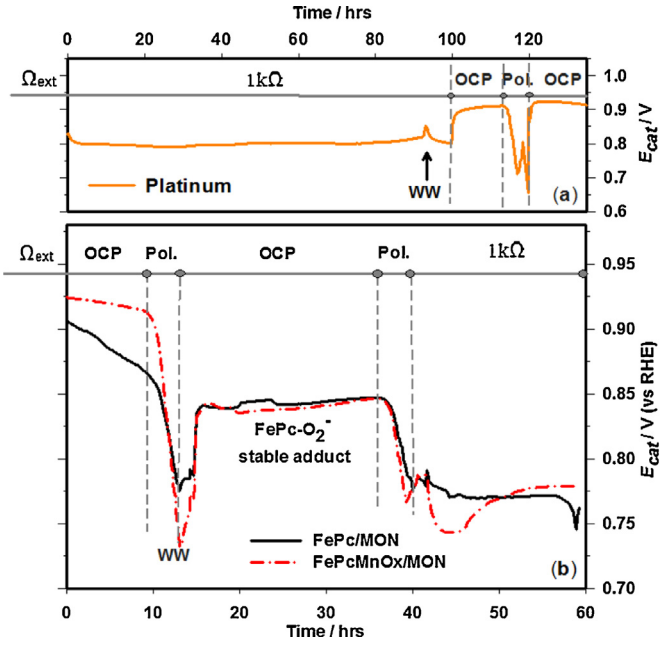

Fig. 4. Cathode potential vs. batch time, in relation to the fixed external resistor; 1 kΩ, Open circuit (OCP) or stepwise decrease in external resistor (Pol.). New electrodes at t = 0. Electrode materials of (a) Pt/C and (b) FePc/MON and FePcMnOx/MON. key; WW = Remove old wastewater, fresh wastewater inserted. Electrolyte; primary clarifier influent 75 %v/v + 25 %v/v PBS stock solution, equivalent 50 mM PBS – pH 7.05, 6.6 mS cm^{-1}.

With a fixed external load, MFCs using artificial wastewaters typically produce a plateau response for V_{cell} if one type of organic carbon source is used [5]. With a fixed external resistor a stable plateau in V_{cell} was not observed for all wastewater cells, indicative of glycolysis or fermentive biotic processes limiting biofilm growth and power MFC output. Batch performances after polarisation curves produced P_{max} of 50.4 mW m^{-2} and 30.2 mW m^{-2} for FePcMnOx/MON and FePc/MON, respectively.

The initial drop in OCP (Fig. 4b) occurs when acidified Nafion binder requires neutralisation, and time is required for O_2 percolate through the FePc films re-ordering them [70], a process which controls the potential. After polarisation, an equilibrium OCP of E = 0.842 V is recorded in PBS media for thin film experiments on FePc electrodes [20]. In wastewater (Fig. 4b), a stable OCP response at E = 0.842 V is seen over 18 h. The stable FePc-oxo adduct described by Zagal et al. [71], controls this potential in both media. In mixed potential theory, a consistent OCP after addition of contaminants (wastewater) suggest selectivity for the dominant reaction prior to contaminant addition. This observation establishes that un-pyrolysed FePc is inert to organic cross-over

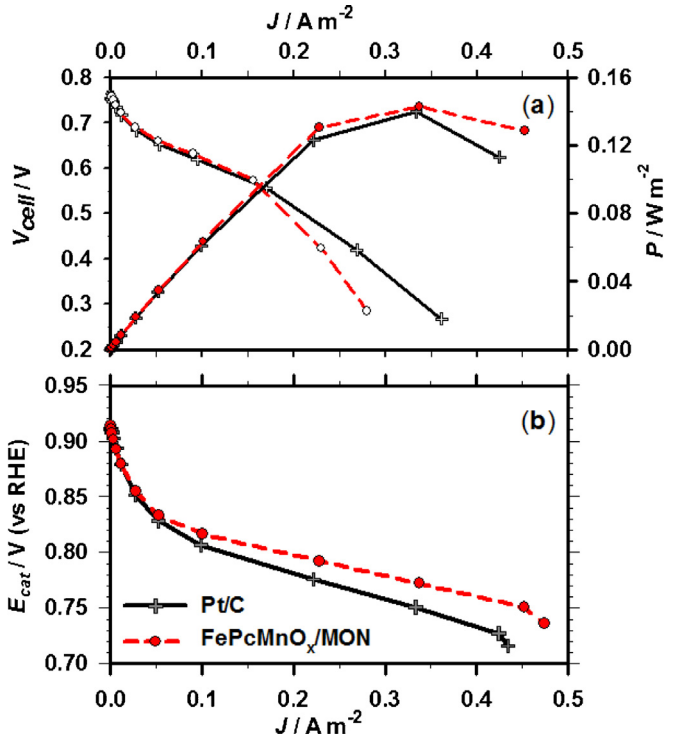

Fig. 5. Steady state polarization curves showing (a) V_{cell} vs. J and P vs. J and, (b) the corresponding cathode potentials, E_{cat} vs. J. Air cathodes; Pt/C, FePc/MON and FePcMnOx/MON. Electrolyte; 50 mM PBS buffered primary clarifier influent, pH 7.05, 6.6 mS cm^{-1}.

reactions in the wastewater used. In contrast, Pt is severely affected by parasitic oxidation reactions in buffered wastewater; in Fig. 4 the stable OCP = 0.922 V is 0.1 V lower than that in pure buffer (E = 1.02 V) [20,72], indicating significant cross-over reactions catalysed on the Pt surface [72]. The observations of Pt and FePc show agreement with the ORR selectivity study of Harnisch et al. on pyrolysed FePc [72]. In Fig 4b, the OCP of FePc/MON and FePcMnOx/MON cathodes appear consistent. This indicates organic cross-over reactions are not catalysed by the MnOx, which would result in a lower OCP in the composite. This observation applies to both the synthesised MnOx and the passivized forms generated from cathodic polarisation (discussed in Section 3.2), making the material suitable for wastewater applications.

Steady state polarisation was taken at t = 9 and 12.5 h, see Fig. 4b, and the results are shown in Fig. 5. P_{max} occurs at external resistance 1 kΩ for all electrodes. Polarisation in wastewater produced P_{max} of 143 mW m^{-2} for FePcMnOx/MON, 66 mW m^{-2} for FePc/MON and 140 mW m^{-2} for Pt, see Fig. 5a.

MFC's exhibited anode limitation at high current (>0.4 A m^{-2}) due to limiting biofilm size incurring metabolic limitation. This conclusion arises from a comparison of the linear E_{cat}–J plot in Fig. 5b to the V_{cell} deterioration in the 0.15–0.4 A m^{-2} current region in Fig. 5a. Prior to this metabolically limiting anode current the V_{cell} follows the order FePcMnOx/MON > Pt/C > FePc/MON. Application of iR-drop correction to the data in Fig. 5b ($R_s = L/(A\kappa)$ = 9.65 Ω) does not significantly alter the plot, decreasing E_{cat} by only 3.1 mV at 0.3 A m^{-2}. Intriguingly, the linear drop (0.15–0.4 A cm^{-2}) is due to a cathode surface resistance which is invariant of potential. This eliminates polarisation resistances as a cause [73]. This behaviour is observed during electrochemical impedance spectroscopy investigation on FePc air cathodes [20], akin to resistance from a highly charged double layer or a surface state resistance. This resistance was smaller in both FePc based (1800 Ω cm^2) electrodes in comparison to the linear drop region with Pt (2300 Ω cm^2).

In the activation region, a linear tafel plot was obtained from Fig. 5b. The $\log_{10}(J)$–E_{cat} produced a linear slope for fresh cathodes of FePcMnOx/MON and Pt/C of $-b_c$ = 0.07 V dec^{-1} (R^2 = 0.994) and $-b_c$ = 0.105 V dec^{-1} (R^2 = 0.999), respectively, from 0.03 to 0.3 A m^{-2}. While these Tafel slopes differ from those obtained in pure PBS this indicates that the complex nature of the electrolyte causes a shift in reaction bottlenecks to an earlier step in the reaction [20]. The linear Tafel plot of the MnOx electrode shows an absence of other concurrent reactions occurring under kinetic control, an observation consistent with the lack of a mixed potential observed in Fig. 4.

4. Conclusions

This work describes the preparation of a composite oxygen reduction catalyst of iron phthalocyanine and mineralised manganese(III) and (IV) oxides. To the author's knowledge, this is the first attempt to analyse ORR activity of an iron or cobalt macrocycle/manganese oxide composite in neutral pH medium. Successful loading of the catalyst was verified and quantified by XPS. Although MnOx polymorph chemistry was not influenced by the preceding FePc deposition, the Fe2p spectra showed a shift to higher binding energies associated with higher oxidation states. Quantification showed a similar portion of loaded FePc retained redox activity in both FePc/MON and FePcMnOx/MON, showing co-deposition to be benign to the primary catalyst.

Composite air cathodes and thin films were compared to unmodified FePc/MON in both phosphate and phosphate buffered primary clarifier influent. An improvement in H_2O_2 degradation was established with RRDE, this is particularly apt in conditions where H_2O_2 accumulation may inhibit the catalyst [23] and damage bio-electrochemical reactor components such as membranes. A Pt/C benchmark with a high loading of precious metal (0.5 mg cm^{-2}) produced less cathodic current in half-cells with buffered electrolyte. In addition, this study represents one of the first uses of FePc in buffered primary clarifier influent wastewater, as opposed to buffered nutrient media. The solutes in wastewater were found to have minimal effect on FePc site viability in the short term. With the addition of MnOx the MFC produced 143 mW m^{-2} with the composite air cathode compared to Pt/C producing 140 mW m^{-2}.

The proposal of MnOx as a lone MFC cathode catalyst has been made by several groups. Yet investigations into the stability and cathodic nature of the catalyst have caused some disparity [8,32]. ICP analysis of electrolyte samples showed synthesised MnOx to be stable even after cathodic polarisation, despite neutral pH conditions favouring Mn^{2+} at equilibria [32,34]. A working model of the composite suggests that a high redox balance in the film could maintain MnOx activity. The results suggest admixtures of MnOx with H_2O_2 generating iron phthalocyanines tuned with higher redox potentials (such as Fe-tetrapyridinoporphyrazine [74]) will further improve activity provided the Fe chelates are not gradually decomposed by H_2O_2. Alternatively, highly active quinone's immobilised with MnOx on an inert support or in conductive films could produce highly active cathode designs. Further improvements can be obtained with the use of anion exchange membranes which are widely prescribed for MFC technology and will further abate any Mn^{2+} leaching into treated wastewater, promoting a regenerative mechanism confined to the catalyst layer. At the current state of development, the passivized MnOx retains disproportionation activity after electrochemical aging. Stabilising H_2O_2 sensitive non-precious catalysts and membrane materials produce a barrier to allowing an MFC to operate under environmental conditions without regular maintenance or replacement of components.

Acknowledgements

R. Burkitt thanks EPSRC for a DTA studentship, and the work is supported by EPSRC Supergen-Biological Fuel Cells (EP/H019480/1). Professor Peter Cumpson and the National EPSRC XPS Users' Service (NEXUS) are acknowledged for recording XPS data of catalyst samples.

Appendix A. Supplementary data

Supplementary data associated with this article can be found, in the online version, at http://dx.doi.org/10.1016/j.apcatb.2015.07.010

References

[1] B. Logan, Appl. Microbiol. Biotechnol. 85 (2010) 1665–1671.
[2] E.S. Heidrich, J. Dolfing, K. Scott, S.R. Edwards, C. Jones, T.P. Curtis, Appl. Microbiol. Biotechnol. 97 (2013) 6979–6989.
[3] Y. Feng, W. He, J. Liu, X. Wang, Y. Qu, N. Ren, Bioresour. Technol. 156 (2014) 132–138.
[4] B. Logan, Water Sci. Technol. 52 (2005) 31–37.
[5] S. Cheng, H. Liu, B.E. Logan, Environ. Sci. Technol. 40 (2005) 364–369.
[6] E. HaoYu, S. Cheng, K. Scott, B. Logan, J. Power Sources 171 (2007) 275–281.
[7] F. Zhao, F. Harnisch, U. Schröder, F. Scholz, P. Bogdanoff, I. Herrmann, Electrochem. Commun. 7 (2005) 1405–1410.
[8] I. Roche, K. Katuri, K. Scott, J. Appl. Electrochem. 40 (2010) 13–21.
[9] L. Zhang, C. Liu, L. Zhuang, W. Li, S. Zhou, J. Zhang, Biosens. Bioelectron. 24 (2009) 2825–2829.
[10] N. Duteanu, B. Erable, S.M. Senthil Kumar, M.M. Ghangrekar, K. Scott, Bioresour. Technol. 101 (2010) 5250–5255.
[11] A. Kozawa, V.E. Zilionis, R.J. Brodd, J. Electrochem. Soc. 117 (1970) 1470–1474.
[12] A. Kozawa, V.E. Zilionis, R.J. Brodd, J. Electrochem. Soc. 117 (1970) 1474–1478.
[13] E. Yu, S. Cheng, B. Logan, K. Scott, J. Appl. Electrochem. 39 (2009) 705–711.
[14] J.H. Zagal, Coord. Chem. Rev. 119 (1992) 89–136.
[15] G. Lalande, G. Faubert, R. Côté, D. Guay, J.P. Dodelet, L.T. Weng, P. Bertrand, J. Power Sources 61 (1996) 227–237.
[16] Y. Yuan, J. Ahmed, S. Kim, J. Power Sources 196 (2011) 1103–1106.
[17] Y. Yuan, B. Zhao, Y. Jeon, S. Zhong, S. Zhou, S. Kim, Bioresour. Technol. 102 (2011) 5849–5854.
[18] Y. Yuan, S. Zhou, L. Zhuang, J. Power Sources 195 (2010) 3490–3493.
[19] S. Baranton, C. Coutanceau, E. Garnier, J.M. Léger, J. Electroanal. Chem. 590 (2006) 100–110.
[20] R. Burkitt, Improvement of the Oxygen Reduction Cathodes of Microbial Fuel Cells Designed to Treat Municipal Wastewater, Chemical Engineering and Advanced Materials, University of Newcastle, Newcastle upon Tyne, 2014, p265.
[21] R. Baker, D.P. Wilkinson, J. Zhang, Electrochim. Acta 53 (2008) 6906–6919.
[22] H. Schulenburg, S. Stankov, V. Schunemann, J. Radnik, I. Dorbandt, S. Fiechter, P. Bogdanoff, H. Tributsch, J. Phys. Chem. B 107 (2003) 9034–9041.
[23] R. Chen, H. Li, D. Chu, G. Wang, J. Phys. Chem. C 113 (2009) 20689–20697.
[24] K. Arihara, L. Mao, P.A. Liddell, E. Marino-Ochoa, A.L. Moore, T. Imase, D. Zhang, T. Sotomura, T. Ohsaka, J. Electrochem. Soc. 151 (2004) A2047–A2052.
[25] M. El-Deab, S. Othman, T. Okajima, T. Ohsaka, J. Appl. Electrochem. 38 (2008) 1445–1451.
[26] X.-Y. Xie, Z.-F. Ma, X.-X. Ma, Q. Ren, V.M. Schmidt, L. Huang, J. Electrochem. Soc. 154 (2007) B733–B738.
[27] D. Zhang, D. Chi, T. Okajima, T. Ohsaka, Electrochim. Acta 52 (2007) 5400–5406.
[28] X. Li, B. Hu, S. Suib, Y. Lei, B. Li, J. Power Sources 195 (2010) 2586–2591.
[29] X. Li, B. Hu, S. Suib, Y. Lei, B. Li, Biochem. Eng. J. 54 (2011) 10–15.
[30] X.-W. Liu, X.-F. Sun, Y.-X. Huang, G.-P. Sheng, K. Zhou, R.J. Zeng, F. Dong, S.-G. Wang, A.-W. Xu, Z.-H. Tong, H.-Q. Yu, Water Res. 44 (2010) 5298–5305.
[31] M. Lu, S. Kharkwal, H.Y. Ng, S.F.Y. Li, Biosens. Bioelectron. 26 (2011) 4728–4732.
[32] A. Rhoads, H. Beyenal, Z. Lewandowski, Environ. Sci. Technol. 39 (2005) 4666–4671.
[33] I. Roche, K. Scott, J. Electroanal. Chem. 638 (2010) 280–286.
[34] N. Takeno, National Institute of Advanced Industrial Science and Technology, Research Center for Deep Geological Environments, 2005.
[35] J. Ahmed, H.J. Kim, S. Kim, RSC Adv. 4 (2014) 44065–44072.
[36] A.J. Appleby, M. Savy, J. Electroanal. Chem. 92 (1978) 15–30.
[37] L. Mao, D. Zhang, T. Sotomura, K. Nakatsu, N. Koshiba, T. Ohsaka, Electrochim. Acta 48 (2003) 1015–1021.
[38] N. Ominde, N. Bartlett, X.-Q. Yang, D. Qu, J. Power Sources 195 (2010) 3984–3989.
[39] B. Xu, M.-L. Ye, Y.-X. Yu, W.-D. Zhang, Anal. Chim. Acta 674 (2010) 20–26.
[40] S. Thiagarajan, T.H. Tsai, S.-M. Chen, Int. J. Electrochem. Sci. 6 (2011) 2235–2245.
[41] V. Gomez-Toribio, A.T. Martınez, M.J. Martınez, F. Guillen, Eur. J. Biochem. 268 (2001) 4787–4793.
[42] C.J. Clarke, G.J. Browning, S.W. Donne, Electrochim. Acta 51 (2006) 5773–5784.
[43] S. Bakardjieva, P. Bezdička, T. Grygar, P. Vorm, J. Solid State Electrochem. 4 (2000) 306–313.
[44] P. Aelterman, S. Freguia, J. Keller, W. Verstraete, K. Rabaey, Appl. Microbiol. Biotechnol. 78 (2008) 409–418.
[45] A. Van Der Putten, A. Elzing, W. Visscher, E. Barendrecht, J. Electroanal. Chem. 214 (1986) 523–533.
[46] *N*4-Macrocyclic Metal Complexes, in: J.H. Zagal, F. Bedioui, J.-P. Dodelet (Eds.), 1 ed., Springer, 2011.
[47] A. Ciszewski, G. Milczarek, Talanta 61 (2003) 11–26.
[48] G.V. Shteinberg, A.V. Dribinsky, I.A. Kukushkina, L.N. Mokorousov, V.S. Bagotzky, J. Electroanal. Chem. 180 (1984) 619–637.
[49] D.B. Sepa, M.V. Vojnovic, A. Damjanovic, Electrochim. Acta 26 (1981) 781–793.
[50] A.A.M. Daifullah, S.M. Yakout, S.A. Elreefy, J. Hazard. Mat. 147 (2007) 633–643.
[51] I. Roche, E. Chaînet, M. Chatenet, J. Vondrák, J. Phys. Chem. C 111 (2007) 1434–1443.
[52] A. Muthukrishnan, Y. Nabae, T. Hayakawa, T. Okajima, T. Ohsaka, Catalysis Sci. Technol. 5 (2015) 475–483.
[53] S. Valarselvan, P. Manisankar, Electrochim. Acta 56 (2011) 6945–6953.
[54] G.S. Szymanski, Z. Karpinski, S. Biniak, A. Swiatkowski, Carbon 40 (2002) 2627–2639.
[55] F. Van Den Brink, W. Visscher, E. Barendrecht, J. Electroanal. Chem. 172 (1984) 301–325.
[56] E. Martin, B. Tartakovsky, O. Savadogo, Electrochim. Acta 58 (2011) 58–66.
[57] E.R. Stadtman, B.S. Berlett, P.B. Chock, Proc. Natl. Acad. Sci. 87 (1990) 384–388.
[58] J.H. Zagal, M.A. Gulppi, G. Cárdenas-Jirón, Polyhedron 19 (2000) 2255–2260.
[59] K. Nilson, Phthalocyanines on Surfaces, Department of Physics, University of Uppsala, Uppsala, 2007.
[60] J. Åhlund, K. Nilson, J. Schiessling, L. Kjeldgaard, S. Berner, N. Mårtensson, C. Puglia, B. Brena, M.a. Nyberg, Y. Luo, J. Chem. Phys. 125 (2006) 034709.
[61] P. García, J.F. Espinal, C. Salinas Martínez de Lecea, F. Mondragón, Carbon 42 (2004) 1507–1515.
[62] J.L. Hueso, J.P. Espinós, A. Caballero, J. Cotrino, A.R. González-Elipe, Carbon 45 (2007) 89–96.
[63] C. Isvoranu, J. Åhlund, B. Wang, E. Ataman, N. Mårtensson, C. Puglia, J.N. Andersen, M.-L.a. Bocquet, J. Schnadt, J. Chem. Phys. 131 (2009) 214,709.
[64] C. Isvoranu, Metal-Organic Complexes at Surfaces, Division of Synchrotron Radiation Research, Lund University, Lund, Sweeden, 2010.
[65] V.Y. Aristov, O.V. Molodtsova, V.V. Maslyuk, D.V. Vyalikh, T. Bredow, I. Mertig, A.B. Preobrajenski, M. Knupfer, Organic Electronics 11 (2010) 1461–1468.
[66] H.W. Nesbitt, D. Banerjee, Am. Minerologist 83 (1998) 305–315.
[67] P. Bezdicka, T. Grygar, B. Klápste, J. Vondrák, Electrochim. Acta 45 (1999) 913–920.
[68] C.J. Matocha, E.A. Elzinga, D.L. Sparks, Environ. Sci. Technol. 35 (2001) 2967–2972.
[69] L. Wang, P. Liang, J. Zhang, X. Huang, Bioresour. Technol. 102 (2011) 5093–5097.
[70] E. Kuzmann, Z. Homonnay, A. Vértes, S. Li, H. Yin, Y. Wei, A. Nath, X. Chen, J. Li, J. Solid State Chem. 170 (2003) 118–123.
[71] J.H. Zagal, S. Griveau, J.F. Silva, T. Nyokong, F. Bedioui, Coord. Chem. Rev. 254 (2010) 2755–2791.
[72] F. Harnisch, S. Wirth, U. Schröder, Electrochem. Commun. 11 (2009) 2253–2256.
[73] F. Zhang, D. Pant, B.E. Logan, Biosens. Bioelectron. 30 (2011) 49–55.
[74] J.H. Zagal, F. Bedioui, J.-P. Dodelet, N4 Macrocyclic Metal Complexes, Springer, 2009.